TiO_2 NANOSTRUCTURED SURFACE COATINGS FOR TETRACYCLINE RELEASE

Angela Gabriela PĂUN[1], Cristina DUMITRIU[1], Nicoleta BADEA[1], Simona POPESCU[1]*

The current study investigates the potential entrapment of tetracycline on the TiO_2 nanostructured surfaces. To achieve this, these nanostructures were created using various methods and conditions. The samples were subjected to characterization for revealing the morphology, wettability, and electrochemical stability. The release capability of the antibiotic was analyzed to highlight the differences among the nanostructures. The results suggest that these substrates are highly suitable for binding tetracycline. The newly developed surfaces, Y-branched TiO_2 nanotubes, can be employed as an intermediate layer for incorporating antibiotics and facilitating local release on surfaces intended for orthopedic and dental implants.

Keywords: TiO_2 nanotubes, Y-branched TiO_2 nanotubes, TiO_2 nanofibers, tetracycline release

1. Introduction

Titanium dioxide nanostructures, such as titania nanotubes (NTs) and TiO_2 nanofibers (NFs) are favorable for surface coating on metallic implants, particularly due to their versatile applications in the field of biomedicine [1-4]. NTs properties include an increase in the total surface area of the implant, enhanced wettability, improved resistance to biological wear, and the introduction of antibacterial features [2, 5]. On the flip side, the porous nature of NTs plays a beneficial role in promoting the regeneration and repair of bones [2, 6-8]. Moreover, NTs have the potential to be integrated with specific drugs and/or proteins [1, 9], enabling precise control over their release in the environment surrounding the implants [2, 10]. Importantly, drug release is not confined to UV reactions; it can be initiated electrically (via voltage-induced catalysis) or, notably, by X-rays. This feature enables *in vivo* treatments of tissue [11]. The manufacturing process for NTs is considered cost-effective and relatively straightforward, with the physicochemical surface properties precisely controlled through specific procedures during

[1] Department of General Chemistry, Faculty of Chemical Engineering and Biotechnologies, National University of Science and Technology POLITEHNICA Bucharest, Romania,
* Corresponding author, e-mail: simona.popescu@upb.ro

electrochemical anodization [1, 12, 13]. These nanotube surfaces provide the advantage of precise diameter adjustment within ^{2}a broad range of 10–250 nm [11, 14]. On the flip side, the porous nature of NTs plays a beneficial role in promoting the regeneration and repair of bones [2, 6-8].

Many research endeavors concentrate on employing one-step anodization to create self-organized and vertically aligned NTs. The two-step anodization technique has been utilized to achieve highly organized NTs [15]. Branched TiO_2 nanotubes are believed to enhance the performance of applications involving nanotubes. Various methods, such as anodization, can be employed to create these branched nanotubes [16]. Previous research groups have achieved this by altering factors like temperature, electrolyte composition, or voltage during the anodization process [16, 17]. In the case of anodic TiO_2 nanotubes, employing the same applied voltage but in different electrolytes during anodization leads to the formation of double-layer nanotube arrays, with branched nanotubes growing beneath the trunk nanotubes [15]. The enhanced performance is attributed to the increased specific surface area of the branched nanotubes compared to their non-branched counterparts [16, 17]. This process typically involves the division of larger-diameter nanotubes (stems) into smaller-diameter branches. Because smaller nanostructures have a higher surface-to-volume ratio, a decrease in the nanotube's diameter may also result in a higher specific surface area. Importantly, this higher specific surface area allows Y-branched NTs to capture more visible light compared to one-dimensional TiO_2 nanotubes of equivalent thickness, all while maintaining the vertically aligned one-dimensional nanostructure. The distinctive aspect of this mechanism lies in its ability to craft multi-stage Y-branched TiO_2 nanotube resembling a 'nano-tree' through precise adjustment of the ramping steps. This unique structure opens up possibilities for intriguing applications [17].

The hierarchical porous tube-like structures of TiO_2 nanofibers have attracted considerable interest in applications such as photocatalysis, sensors, waveguides, and implant biomaterials. This is attributed to their enhanced ability to facilitate mass transport throughout the material and maintain a substantial specific surface area within a reasonable porosity range [18]. TiO_2 nanofibers represent a unique category of biocompatible nanostructured materials extensively employed in the domains of biotechnology and biomedical engineering. Their utilization is driven by their attributes as potent oxidizing agents, chemical inertness, and non-toxic nature [19]. Nanoscale fibers give nanocomposites improved mechanical qualities like high modulus, high tensile strength, and toughness [20]. They also possess qualities like ease of production, low toxicity, enhanced therapeutic efficacy, and high operational efficiency and ability to load drugs [21].

Implants are linked to the occurrence of osteomyelitis, leading to subsequent implant failure. A compelling strategy to mitigate the bacteriological risks associated with implants involves implementing a local drug release system within the implant material, serving as a carrier for drugs like antibiotics [22]. Nowadays, the use of TiO_2 nanostructures in drug delivery systems has become widely popular due to their efficacy in enhancing healing and reducing medical side effects, attributed to their non-toxic nature. Therapeutic drugs find easy incorporation into either TiO_2 nanofibers mats or TiO_2 nanotubular structures. The composition and morphological structures of these structures, influenced by suitable material fabrication techniques, significantly impact the control of drug release. Tetracycline (TE), a hydrophilic antibiotic, is commonly employed to treat and prevent bacterial infections associated with burns, cuts, and surgeries, serving various wound healing purposes [23]. Beyond its antibiotic properties, tetracycline also demonstrates anti-collagenase activity, inhibits bone resorption, possesses anti-inflammatory effects, and fosters the attachment of fibroblasts and connective tissue to root surfaces. Furthermore, tetracycline has been reported to inhibit the quantity and activity of proteinases, making it applicable in the treatment or prevention of diseases associated with proteinase imbalance, such as cancer metastasis, rheumatoid arthritis, periodontitis, and osteomyelitis [22, 24]. Tetracycline loaded nanotubes can prevent bacterial colonization around implants by delivering high concentrations of antibiotics locally without endangering the body. Moreover, the osseous-integrative characteristics of the surface are unaffected [25].

In this study, a tailored two-step anodization approach is applied to produce hierarchically branched TiO_2 nanotubes in various electrolytes. Additionally, TiO_2 nanotubes were also obtained in a single step, and then TiO_2 nanofibers were deposited. The two types of substrates were then compared based on their ability to effectively enable the controlled release of an antibiotic drug, tetracycline. The samples, featuring modified surfaces, underwent morphological and electrochemical assessments, and their capability for controlled drug release was evaluated through UV analysis.

2. Experimental section

2.1 ***Materials***

This investigation used 1 cm × 1 cm pieces of 99.7% pure titanium (Ti) supplied by Alpha Aesar. Utilizing an abrasive paper with varying porosities (320, 800, and 1200, respectively) and a Beta 2 grinder-polisher (Buehler), titanium samples were polished. Following polishing, the Ti samples were cleaned by sonicating them for 15 minutes at room temperature in distilled water, ethanol, and acetone, respectively.

Other reagents: Ethylene glycol – anhydrous (99.8% purity); ammonium fluoride; hydrofluoric acid; sulfuric acid; dimethyl sulfoxide (DMSO); titanium butoxide; glacial acetic acid, N, N-Dimethylformamide (DMF), sodium phosphate dibasic dihydrate, sodium dihydrogen phosphate monohydrate were purchased from Sigma Aldrich. Polyvinylpyrrolidone and isopropanol were provided by Fluka.

2.2 Methods

2.2.1 TiO_2 nanotube structures preparation

Two electrodes were used in the anodizing process: a Ti electrode was attached to the voltage source's positive terminal (the anode) and a Pt electrode was attached to its negative terminal (the cathode) in the electrochemical cell. With a rate of 2 V per 10 seconds, the voltage increased from 0 to the value indicated in Table 1 using a MATRIX MPS-7163 source. After that, it was maintained constant at room temperature.

Table 1

Composition of electrolyte solutions used for anodizing and applied voltage.

Method	Electrolyte composition	Steps	Voltage (V)	Time (h)	Sample name
Anodization to obtain monolayer nanotubes	0.5 wt.% NH_4F + 2 v.% distilled water + EG	Step 1	50	2	**NT_1s**
Anodization to obtain multilayer nanotubes	1 M H_2SO_4 + 0.16 M HF	Step 1	20	2	**NT_2s**
	0.5 wt.% NH_4F + 2 v.% distilled water + EG	Step 2	20	2	

Following anodizing, the modified samples were cleaned with distilled water and calcined at 450°C for two hours.

2.2.2 TiO_2 nanofiber obtained by electrospun

The TiO_2 nanofibers production using electrospun procedure followed the protocol described in the literature [26]. The solution was obtained by hydrolysis of 4 wt.% Titanium Butoxide and 8 wt.% PVP in DMF: isopropanol mixture (mass ratio of 1/1) and 2 wt.% glacial acetic acid. 1 ml of this solution was introduced in a plastic syringe. A syringe pump (model Legato 180 from KDS Scientific USA) was utilized to apply a 0.5 ml/h flow rate of liquid. The power source (PS/EJ30P20 series from Glassman High Voltage Inc.) was used to apply 15 kV between the grounded collector plate and the syringe needle tip for 10 minutes. The distance between the tip of the syringe needle and the collector plate was fixed to 10 cm. **Ti** and **NT_1s** samples were fixed on the collector to obtain **NF** and **NT-1s/NF** samples.

The Ti samples coated with nanofibers were kept overnight inside a fume hood at room temperature to fully hydrolyze the Titanium Butoxide from the nanofibers. The nanofibers are then pyrolyzed at 500 °C for 4 hours (to allow complete elimination of PVP and other organic components from the fibers as well as for TiO_2 crystallization).

2.2.3 Tetracycline incorporation

Firstly, a 4 g/L concentration of tetracycline solution was prepared for antibiotic embedding into TiO_2 nanostructure. The solubilization process used a 3:1 ratio of ethanol to distilled water due to the antibiotic's low water stability. The modified samples (NT_1s, NF, NT_1s/NF, and NT_2s) were submerged in 10 mL of tetracycline solution at room temperature for 48 hours. These samples were named **NT_1s/TE**, **NF/TE**, **NT_1s/NF/TE** and **NT_2s/TE**.

2.2.4. Characterization

Surface morphology examination was performed employing a field emission scanning electron microscope FEI/Philips XL-30 (equipped with EDAX annex). The surface wettability was studied using the Sesile Drop method and a CAM 100 Optical Contact Angle Meter type equipment. The microstructure was examined using a microscope attached to a Tukon's Wilson Hardness system. The electrochemical characterization of the modified samples was performed in a cell with three electrodes: working electrode is a Ti or coated Ti electrode, reference electrode is an Ag/AgCl/3M KCl electrode (Methrom), and counter electrode was a 2 mm Pt rod electrode (Methrom). The electrochemical experiments were performed in simulated Fusayama saliva (0.9 g/L KCl, 0.4 g/L NaCl, 0.69 g/L NaH_2PO_4, 0.795 g/L $CaCl_2 \cdot H_2O$, 1 g/L urea) using a potentiostat/galvanostat model PGSTAT 302N (Autolab) and Nova 1.10 software.

3. Results and discussion

3.1 SEM analysis

The samples were morphologically examined to confirm the nanostructured surfaces and the presence of tetracycline [27]. The SEM images of the nanostructured modified materials with and without tetracycline are shown in Fig. 1. The SEM images of titanium samples modified by nanofibers (NF) are seen in Fig. 1a. The nanofibers exhibit a random and uniform distribution throughout the surface of the sample. They possess an average diameter of approximately 30 nm and their surface displays a smooth and uninterrupted structure without beds or agglomerations.

The SEM images of the anodized samples in one step, over which nanofibers were deposited (NT_1s/NF), are shown in Fig. 1b, c. It is evident that the nanofibers are evenly dispersed throughout the whole surface of the nanotubes

and have a size of around 60 nm, Fig. 1b. In Fig. 1c it is observed that the TiO_2 nanotubes have a porous structure, with ordered pores similar to "honeycombs". They are not completely covered with nanofibers. When the nanofibers are deposited on the nanotubular surface, they become coarser.

In Fig. 1d-e, the SEM images of the NF and NT_1s/NF samples functionalized with tetracycline are presented. After loading the tetracycline, the morphology of TiO_2 nanofibers was not influenced.

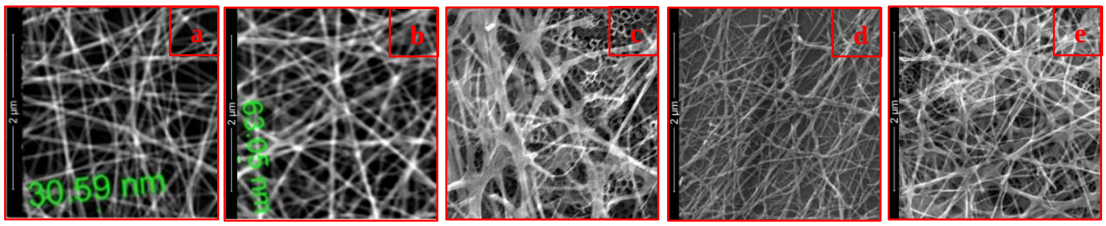

Fig. 1. SEM images: a. NF; b, c. NT_1s/NF; d. NF/TE; e. NT_1s/NF/TE

Fig. 2 shows the SEM images of the samples anodized in two steps functionalized or not with tetracycline (NT_2s and NT_2s/TE). A double-layer structure is visible in Fig. 2a, consisting of two types of layers: one with higher outer diameters of around 160 nm and one with the smaller diameter of about 100 nm. From the Fig. 2a inset, the inner diameter of the TiO_2 nanotubes is about 60 nm. They are also organized, vertically aligned, and dispersed uniformly. When viewed from above, these nanotubes have a porous structure with organized pores, comparable to "honeycombs". The NT_2s sample exhibits a well-organized, branching morphology, with outer diameter values between 78 and 165 nm.

Fig. 2b presents SEM images of the NT_2s/TE sample. It can be observed that tetracycline does not influence to much the morphology of the nanotubes. By incorporating tetracycline into the nanotubes, the diameter is reduced from 60 nm for the NT_2s sample to around 30 nm for the NT_2s/TE sample.

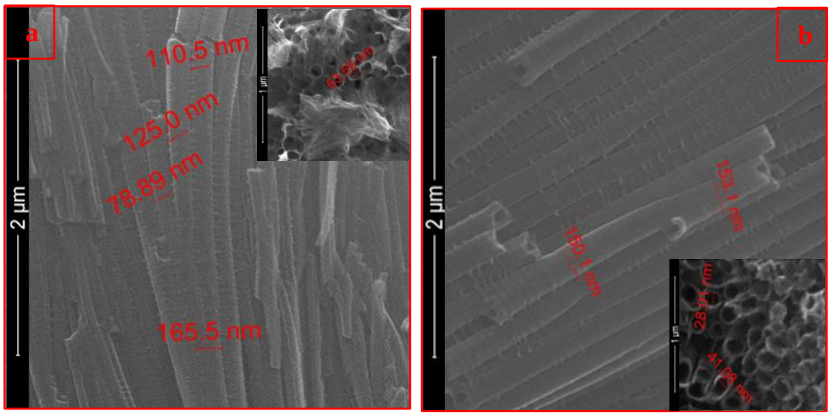

Fig. 2. SEM images of anodized samples: a. NT_2s; b. NT_2s/TE

3.2 Wettability and surface energy

Drops (100 μL) of three different solvents, water, EG, and DMSO, were deposited on the sample's surface using a syringe. The contact angle was measured at least three times, in various parts of the sample surface, at room temperature, and in daylight.

Wettability, charge and surface chemistry are important characteristics for tissue-implant interaction. For medical devices, the hydrophilicity of the implant interface is essential because it encourages cell adhesion and proliferation on the surface. The contact angle can be generated when a drop of liquid falls on a solid surface due to a balance of forces that expresses itself at the boundary of the three phases (liquid, solid, and vapor). It is defined by the intersection of the solid surface and the line indicating the tangent to the drop's contour.

The Ti substrate is the least hydrophilic of the samples obtained, as demonstrated by the contact angle of 65º vs. water (<90º). The contact angle is reduced due to the nanostructuring of the Ti surface. As a result, the water contact angle value dropped to 17º for the NF sample, to 24º for the NT_2s and 29º for the NT_1s/NF sample. The contact angle slightly changes when tetracycline is encapsulated. These have the following values: 20º for NF/TE, 25º for NT_2s/TE, and 18º for NT_1s/NF/TE.

Thus, tetracyline loading increased the contact angle for NF sample and NT_2s wich is consitent with observations made in other studies [25]. Thus, all modified surfaces samples showed a strong hydrophilic character. Protein attachment, osseointegration, and bone interaction are all facilitated by the implant surface's increased wettability. Consequently, the results of the wettability assay show that these samples have excellent hydrophilicity for use in implant applications [28]. The surface energy was in all cases higher than 30 mJ/m^2. According to the literature, materials with this surface energy have a good interaction with cells [29].

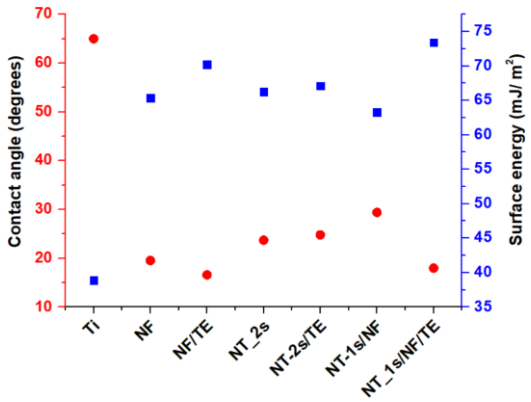

Fig. 3. Water contact angle and surface energy

3.3 Vickers hardness

This approach is based on the application of a force to a pyramidal diamond penetrator with a square base.

Vickers hardness (HV) was determined for the examined samples by conducting five indentations on each sample type. (Fig. 4). As a result, the typical hardness value for each sample was calculated as the average of the five indentations' results. Fig. 4 shows that the changed samples have lower hardness values than the Ti substrate, which is most likely related to the porous morphology observed in the SEM pictures. However, the Vickers hardness values observed are comparable to other literature research on similar samples in terms of surface change [30, 31].

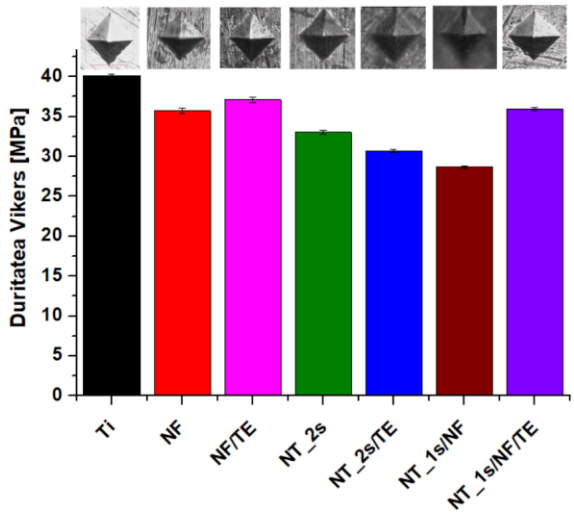

Fig. 4. Vickers harness

3.4 Electrochemical characterization

3.4.1 Tafel analysis

The Tafel polarization curves were recorded in the range of ± 150 mV versus the OCP to obtain the cathodic and anodic branches of the potentiodynamic polarization curves under ambient conditions, with a scanning rate of 2 mV/s. Additionally, electrochemical impedance spectra (EIS) were recorded at room temperature, at the voltage in open circuit, and with an amplitude (AC) of 10 mV within the frequency range of 0.1 - 10^5 Hz.

Tafel diagrams are used to determine the corrosion parameters of the material, which are necessary since the samples are utilized as implantable surfaces immersed in a physiological environment, a corrosive environment. The method is based on anodic and cathodic polarization measurements, with the corrosion rate calculated by the intersection of the anodic and cathodic tangents [32].

The corrosion parameters were calculated using software: corrosion potential (V), corrosion current (A), corrosion current density (A/cm^2), and corrosion rate (mm/year). Table 2 presents the results.

According on the Tafel diagram (Fig. 5) and the data in Table 2, it can be concluded:

- The Ti substrate has the most electronegative value of the corrosion potential, and as a consequence, the highest corrosion rate, 0.0102 mm/year.
- When the surface is covered with TiO_2 nanotubes (NT) or nanofibers (NF), the corrosion potential shifts toward more electropositive values, showing cathodic behavior. The corrosion potential of functionalized samples is similar to that of drug-free samples.
- The coated samples had a considerably lower current density when compared to Ti which made the coated Ti samples more resistant to corrosion because of a passive film formed in all coated samples.
- Because titanium oxide has the properties of a semi-conductor, it acts as a protective layer on pure titanium, stopping the movement of titanium ions and oxygen ions. This makes the corrosion rate go down. The corrosion rate is even more reduced when the changed samples are immersed in tetracycline.

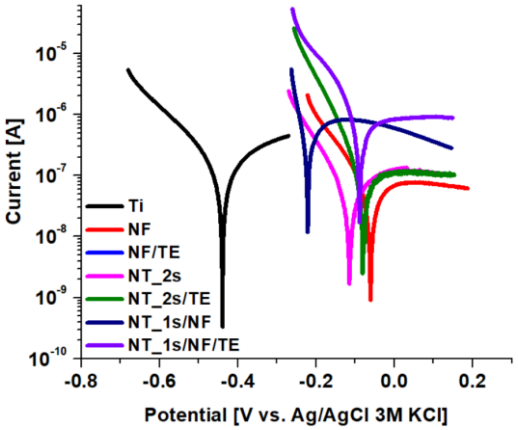

Fig. 5. Tafel diagrams for modified samples

Table 2

Corrosion parameters obtained by Tafel diagrams

Samples	Corrosion potential (V)	Corrosion current density (A/cm^2)	Corrosion rate (mm/year)
Ti	-0.44	$11.7 \cdot 10^{-7}$	$10 \cdot 10^{-3}$
NF	-0.09	$2 \cdot 10^{-7}$	$2.2 \cdot 10^{-3}$
NF/TE	-0.08	$4.3 \cdot 10^{-7}$	$1.7 \cdot 10^{-3}$
NT_2s	-0.12	$3.1 \cdot 10^{-7}$	$2.6 \cdot 10^{-3}$

NT-2s/TE	-0.08	$3.3 \cdot 10^{-7}$	$2 \cdot 10^{-3}$
NT_1s/NF	-0.06	$7.2 \cdot 10^{-7}$	$6.2 \cdot 10^{-3}$
NT_1s/NF/TE	-0.08	$1.8 \cdot 10^{-7}$	$1.5 \cdot 10^{-3}$

3.4.2 Impedance diagrams

Electrochemical impedance spectroscopy (EIS) aims to simulate the real process from the contact between the electrode and the corrosive medium, when the experimental data are introduced into the equivalent electrical circuit. EIS is a helpful analysis that provides information about the processes at the interface, making it valuable for both studying the structure of the electric double layer and estimating charge transfer parameters. This analysis can be used to learn more about the mass transport rate and charge transfer rate of the electroactive species [33].

The Nyquist diagram for modified surface samples is shown in Fig. 6a. First deduced observations are that all coated surfaces are more stable and have higher resistivity than Ti samples. The equivalent circuits that were utilized to fit the data are shown in Fig. 6b–c. The first circuit (Fig. 6b) was used for the untreated titanium. A more complex circuit, shown in Fig. 6c, was used for each coated sample. The behaviour of the nanostructure surface in terms of non-ideal capacitance was explained by the constant phase elements (CPEs). Chi-square value obtained ranged from 0.01 to 0.08, indicating a high level of agreement between the equivalent circuit and the data.

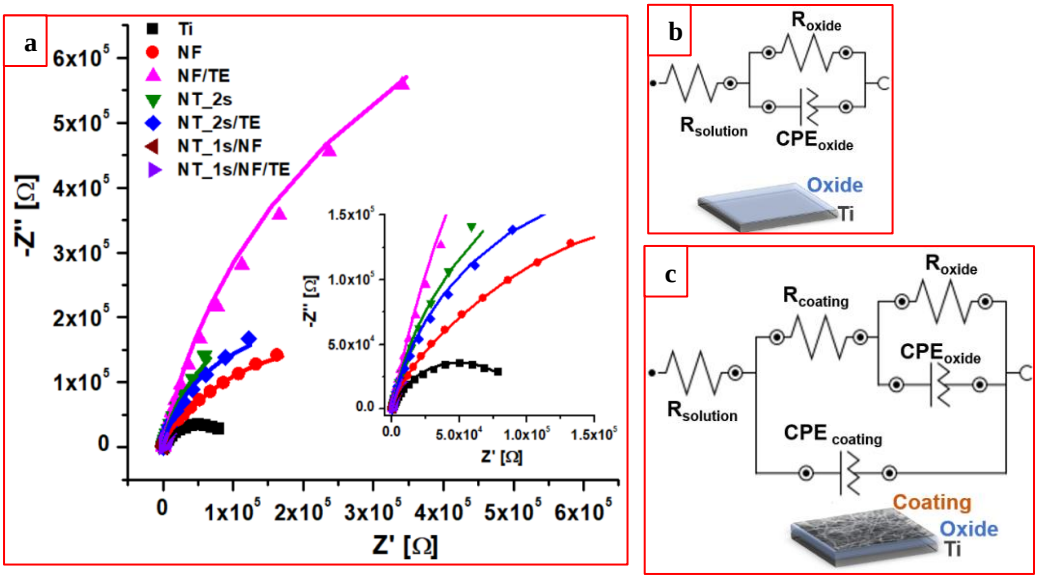

Fig. 5. a) EIS diagram for modified samples b) Equivalent circuits used to fit the EIS data for Ti and c) Circuits used to fit EIS data for coated samples

Table 3 shows the electrical parameters that have been obtained with the Nova software. The solution resistance of all the examined samples is around 300 Ω, due to the similarity of the saline solution and testing conditions. The Ti sample had the greatest susceptibility to corrosion, with a smaller semicircle diameter than the other coated samples, as shown by Nyquist plot in Fig. 5a.

As seen in Table 3, the nanostructures surfaces exhibit a greater resistance of the compact oxide layer (R_{oxide}) in comparison to the pure Ti surfaces. The values exhibit a strong correlation with the Tafel diagram findings, which indicate that the modified Ti samples' corrosion rates were lower than those of the pure Ti sample.

It is noticed that the coating resistivity increases just by adding tetracycline to the nanostructured surfaces. This indicates that all sample with therapeutic agent has enhanced corrosion stability showing that there is an increase in the difficulty of charge transfer across the electrode-solution interface.

CPE is described by the variables Y_0 and N representing the admittance of an ideal capacitance and an empirical constant, respectively. The empirical constant N takes values between 0 and 1. The exponential factor N in the CPE equation represents the departure from the theoretical capacitance. When N is equal to 0, the CPE exhibits characteristics like that of a pure resistor, with Y0 being equal to R. On the other hand, when n is equal to 1, the CPE behaves like a pure capacitor. It is possible to conclude that every sample has a pseudocapacitive character based on the N values between 0.7 and 0.99.

Table 3

Electrical parameters obtained from fitted EIS

Parameter/ Sample	R_S (Ω)	$R_{coating}$ (Ω)	$CPE_{coating}$		R_{oxide} (Ω)	CPE_{oxide}		X^2
			Y_0 ($S*s^n$)	N		Y_0 ($S*s^n$)	N	
Ti	299	-	-	-	$99.1\cdot10^3$	$4.47\cdot10^{-5}$	0.80	0.02
NF	300	$142\cdot10^3$	$8.90\cdot10^{-6}$	0.85	$294\cdot10^3$	$1.18\cdot10^{-5}$	0.73	0.01
NF/TE	332	$843\cdot10^3$	$8.5\cdot10^{-6}$	0,89	$956\cdot10^3$	$67.3\cdot10^{-5}$	0.94	0.02
NT_2s	334	$177\cdot10^3$	$71.2\cdot10^{-6}$	0.89	$350\cdot10^3$	$1.33\cdot10^{-5}$	0.99	0.05
NT_2s/TE	362	$414\cdot10^3$	$34.9\cdot10^{-6}$	0.89	$996\cdot10^3$	$11\cdot10^{-5}$	0.99	0.03
NT_1s/NF	291	$160\cdot10^3$	$40\cdot10^{-6}$	0.75	$300\cdot10^3$	$7.9\cdot10^{-5}$	0.71	0.01
NT_1s/NF/TE	336	$221\cdot10^3$	$395\cdot10^{-6}$	0.88	$301\cdot10^3$	$11\cdot10^{-5}$	0.94	0.08

4. *In vitro* tetracycline release

In order to perform release studies, samples of NF, NT_1s/NF, and NT_2s were submerged in a solution containing 4 g/L of tetracycline for 48 hours. Following that, the samples were then immersed in a 10 mL PBS (pH = 7.4). Using UV-VIS spectrophotometer at a wavelength (λ) of 363 nm, the quantity of drug released over time in the PBS solution was determined.

The quantity of tetracycline released was determined using a calibration curve with a correlation coefficient (R^2) of 0.9992 and a linear regression equation of y = 0.0303x+0.0514 at a tetracycline concentration ranging from 4 to 20 mg/L.

Fig. 6 shows that the drug is rapidly released in the first 8 hours. Tetracycline-modified nanostructured materials release the antibiotic slowly between 20 and 78 hours.

When comparing the three different sample types with tetracycline, NT_2s/TE (25.14%) and NT_1s/NF/TE (32.90%) samples exhibit a slower release than sample NF/TE (48 %). This behaviour can be explained by the controlled morphology of nanotubes, as contrast to the uncontrollable morphology of nanofibers. The smaller diameter and organized structure of the two-step nanotube samples cause a slower release.

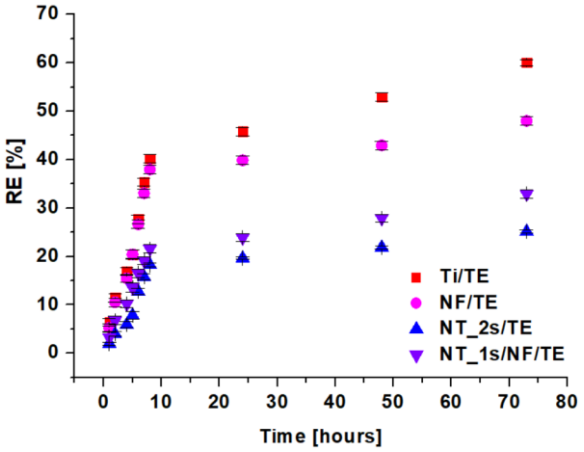

Fig. 6. Tetracycline drug release.

The *in vitro* tetracycline release study data were adjusted using many kinetic models in order to investigate the release kinetics and determine the drug release mechanism.

Table 4.

Kinetic parameters

Samples	Zero order		First order		Higuchi		Peppas-Korsmeyer			Hixson-Crowell	
	R^2	k_0	R^2	k_1	R^2	k_2	R^2	k_3	n	R^2	k_4
Ti/TE	0.965	4.75	0.944	0.029	0.970	9.82	**0.991**	1.762	0.567	0.990	0.003
NF/TE	0,977	4,594	0,960	0,059	0,930	17,27	**0,979**	1,642	0,546	0,956	0,007
NT_2/TE	0,941	2,345	0,933	0,026	0,877	8,720	**0,954**	0,602	0,480	0,932	0,003
NT_1s/NF/TE	0,990	2,581	0,970	0,029	0,970	9,827	**0,991**	1,211	0,465	0,990	0,003

Tetracycline's in vitro release kinetics for each sample types were examined using various models, and the results showed that the drug's release fits the Peppas-Korsmeyer model.

Finally, the encapsulation of tetracycline in TiO_2 nanotubes obtained in two steps (NT_2s/TE) is favorable due to the drug's slow release, which ensures a decrease in adverse effects as well as a prolonged therapeutic impact. Sample is also hydrophilic in nature, showed a low corrosion rate at polarization test and increased corrosion resistance at EIS test being suitable to be used as coating for implant materials.

5. Conclusions

The titanium surface was modified with TiO_2 nanostructures by anodizing and electrospun methods. The resulting nanostructured Ti samples, featuring TiO_2 nanotubes and nanofibers, were further functionalized with an active compound, TE. The surfaces, thus modified, were characterized for morphology, wettability, electrochemical stability, and antibiotic release.

The TE incorporation into these nanostructures decreases contact angle values, suggesting potential enhancing for cell adhesion. Compared to untreated titanium, all modified samples exhibit improved corrosion resistance. Our study indicates that NT_1s/NF or NT_2s can be used to fix TE on the Ti surface.

Furthermore, NT_2s exhibits enhanced tetracycline delivery effectiveness with time, qualifying these materials for local drug delivery applications.

R E F E R E N C E S

[1]. *M.F. Kunrath, R. Hubler, R.S. Shinkai, E.R. Teixeira*. Application of TiO2 nanotubes as a drug delivery system for biomedical implants: a critical overview. ChemistrySelect. 2018;3(40):11180-9.

[2]. *S. Jafari, B. Mahyad, H. Hashemzadeh, S. Janfaza, T. Gholikhani, L. Tayebi*. Biomedical Applications of TiO(2) Nanostructures: Recent Advances. International journal of nanomedicine. 2020;15:3447-70.

[3]. *S. Liu, X. Chen, M. Yu, J. Li, J. Liu, Z. Xie, F. Gao, Y. Liu*. Applications of Titanium Dioxide Nanostructure in Stomatology. Molecules. 2022;27(12):3881.

[4]. *R. Mydin, R. Hazan, M.F. FaridWajidi, S. Sreekantan*. Titanium dioxide nanotube arrays for biomedical implant materials and nanomedicine applications: IntechOpen Ltd. London, UK; 2018.

[5]. *D. Portan, K. Papaefthymiou, C. Pirvu, G. Papanicolaou, I. Demetrescu*. MANUFACTURING AND CHARACTERIZATION OF TiO (2) NANOTUBES ON PURE

TITANIUM SURFACES FOR ADVANCED BIOMEDICAL APPLICATIONS. UPB Buletin Stiintific, Series B: Chemistry and Materials Science. 2011;73(2):181-96.

[6]. *Q. Wang, J.-Y. Huang, H.-Q. Li, A.Z.-J. Zhao, Y. Wang, K.-Q. Zhang, H.-T. Sun, Y.-K. Lai*. Recent advances on smart TiO2 nanotube platforms for sustainable drug delivery applications. International journal of nanomedicine. 2017:151-65.

[7]. *S. Liu, L. Zhang, Z. Li, F. Gao, Q. Zhang, A. Bianco, H. Liu, S. Ge, B. Ma*. Materials-Mediated In Situ Physical Cues for Bone Regeneration. Advanced Functional Materials. 2023:2306534.

[8]. *X. Wen, J. Wang, X. Pei, X. Zhang*. Zinc-based biomaterials for bone repair and regeneration: Mechanism and Application. Journal of Materials Chemistry B. 2023.

[9]. *M. Bariana, J.A. Kaidonis, D. Losic, S. Ranjitkar, P.J. Anderson*. Titania nanotube-based protein delivery system to inhibit cranial bone regeneration in Crouzon model of craniosynostosis. International journal of nanomedicine. 2019;14:6313-24.

[10]. *S. Long, J. Zhu, Y. Jing, S. He, L. Cheng, Z. Shi*. A Comprehensive Review of Surface Modification Techniques for Enhancing the Biocompatibility of 3D-Printed Titanium Implants. Coatings. 2023;13(11):1917.

[11]. *P. Roy, S. Berger, P. Schmuki*. TiO2 nanotubes: synthesis and applications. Angewandte Chemie International Edition. 2011;50(13):2904-39.

[12]. *D. Khudhair, A. Bhatti, Y. Li, H.A. Hamedani, H. Garmestani, P. Hodgson, S. Nahavandi*. Anodization parameters influencing the morphology and electrical properties of TiO2 nanotubes for living cell interfacing and investigations. Materials Science and Engineering: C. 2016;59:1125-42.

[13]. *B.G. Aliabadi, N. Gilani, J.V. Pasikhani, A.E. Pirbazari*. Boosting the photoconversion efficiency of TiO2 nanotubes using UV radiation-assisted anodization as a prospective method: An efficient photocatalyst for eliminating resistant organic pollutants. Ceramics International. 2020;46(12):19942-51.

[14]. *S. Reghunath, D. Pinheiro, S.D. Kr*. A review of hierarchical nanostructures of TiO2: Advances and applications. Applied Surface Science Advances. 2021;3:100063.

[15]. *B. Chen, K. Lu*. Hierarchically Branched Titania Nanotubes with Tailored Diameters and Branch Numbers. Langmuir. 2012;28(5):2937-43.

[16]. *A. Ashari, D.J. Leclere, G. Kawamura, H. Muto, A. Matsuda*. Study of branched TiO2 nanotubes and their application to dye sensitized solar cells. Journal of the Ceramic Society of Japan. 2014;122(1430):886-8.

[17]. *V.C. Anitha, A.N. Banerjee, S.W. Joo, B.K. Min*. Barrier-oxide layer engineering of TiO2 nanotube arrays to get single- and multi-stage Y-branched nanotubes: Effect of voltage ramping and electrolyte conductivity. Materials Science and Engineering: B. 2015;195:1-11.

[18]. *S.P. Adhikari, H.R. Pant, H.M. Mousa, J. Lee, H.J. Kim, C.H. Park, C.S. Kim*. Synthesis of high porous electrospun hollow TiO2 nanofibers for bone tissue engineering application. Journal of Industrial and Engineering Chemistry. 2016;35:75-82.

[19]. *P. Pascariu, A. Airinei, F. Iacomi, S. Bucur, M.P. Suchea*. Chapter 12 - Electrospun TiO2-based nanofiber composites and their bio-related and environmental applications. In: Dinca, V., Suchea, M.P., editors. Functional Nanostructured Interfaces for Environmental and Biomedical Applications: Elsevier; 2019. p. 307-21.

[20]. *D. Khademi, H. Ezatpour, Y. Huo*. The effect of electrospinning time on the structure and mechanical properties of TiO2 continuous nanofibers reinforced aluminum matrix composites. Ceramics International. 2023;49(21):33804-17.

[21]. *A. Purohit, P.K. Panda*. Thread of hope: Weaving a comprehensive review on electrospun nanofibers for cancer therapy. Journal of Drug Delivery Science and Technology. 2023;89:105100.

[22]. *Z.R. Domingues, M.E. Cortés, T.A. Gomes, H.F. Diniz, C.S. Freitas, J.B. Gomes, A.M.C. Faria, R.D. Sinisterra*. Bioactive glass as a drug delivery system of tetracycline and tetracycline associated with β-cyclodextrin. Biomaterials. 2004;25(2):327-33.

[23]. *H.J. Haroosh, Y. Dong, K.-T. Lau*. Tetracycline hydrochloride (TCH)-loaded drug carrier based on PLA:PCL nanofibre mats: experimental characterisation and release kinetics modelling. Journal of Materials Science. 2014;49(18):6270-81.

[24]. *W. Shao, H. Liu, S. Wang, J. Wu, M. Huang, H. Min, X. Liu*. Controlled release and antibacterial activity of tetracycline hydrochloride-loaded bacterial cellulose composite membranes. Carbohydrate Polymers. 2016;145:114-20.

[25]. *L. Sun, J. Xu, Z. Sun, F. Zheng, C. Liu, C. Wang, X. Hu, L. Xia, Z. Liu, R. Xia*. Decreased Porphyromonas gingivalis adhesion and improved biocompatibility on tetracycline-loaded TiO(2) nanotubes: an in vitro study. International journal of nanomedicine. 2018;13:6769-77.

[26]. *C. Dumitriu, A.B. Stoian, I. Titorencu, V. Pruna, V.V. Jinga, R.-M. Latonen, J. Bobacka, I. Demetrescu*. Electrospun TiO2 nanofibers decorated Ti substrate for biomedical application. Materials Science and Engineering: C. 2014;45:56-63.

[27]. *J. Goldstein, D.E. Newbury, P. Echlin, D.C. Joy, A.D. Romig Jr, C.E. Lyman, C. Fiori, E. Lifshin*. Scanning electron microscopy and X-ray microanalysis: a text for biologists, materials scientists, and geologists: Springer Science & Business Media; 2012.

[28]. *A. Ahangari, A. Mokhtarzade, M. Mahmoodi*. In vitro tribological behavior and corrosion resistance of SiO2/TiO2/ZrO2 coatings formed on the tantalum substrate using plasma electrolytic oxidation for orthopedic implant applications. Materials Chemistry and Physics. 2023;308:128210.

[29]. *C. Dumitriu, M. Popescu, C. Ungureanu, C. Pirvu*. Antibacterial efficiencies of TiO2 nanostructured layers prepared in organic viscous electrolytes. Applied Surface Science. 2015;341:157-65.

[30]. *G. Khanna, I. Aparna*. Comparison of microhardness of three different types of acrylic artificial denture teeth: An in vitro study. Journal of Orofacial Research. 2013:181-5.

[31]. *I. Villenas, B.L. Rivas, C. Torres, C. Campos, B.F. Urbano*. Effect of functionalized trititanate nanotubes on the properties of crosslinked cationic polymer nanocomposite. Polymer International. 2015;64(9):1121-7.

[32]. *A.J. Bard, L.R. Faulkner, J. Leddy, C.G. Zoski*. Electrochemical methods: fundamentals and applications: Wiley New York; 1980.

[33]. *A. Lasia*. Electrochemical impedance spectroscopy and its applications. Modern aspects of electrochemistry: Springer; 2002. p. 143-248.